Two-photon spiral imaging with correlated orbital angular momentum states

David S. Simon[1,2] and Alexander V. Sergienko[1,3,4]

[1]*Department of Electrical and Computer Engineering, Boston University, 8 Saint Mary's Street, Boston, Massachusetts 02215, USA*

[2]*Department of Physics and Astronomy, Stonehill College, 320 Washington Street, Easton, Massachusetts 02357, USA*

[3]*Photonics Center, Boston University, 8 Saint Mary's Street, Boston, Massachusetts 02215, USA*

[4]*Department of Physics, Boston University, 590 Commonwealth Avenue, Boston, Massachusetts 02215, USA*

(Received 3 November 2011; published 17 April 2012)

The concept of correlated two-photon spiral imaging is introduced. We begin by analyzing the joint orbital angular momentum (OAM) spectrum of correlated photon pairs. The mutual information carried by the photon pairs is evaluated, and it is shown that when an object is placed in one of the beam paths the value of the mutual information is strongly dependent on object shape and is closely related to the degree of rotational symmetry present. After analyzing the effect of the object on the OAM correlations, the method of correlated spiral imaging is described. We first present a version using parametric down-conversion, in which entangled pairs of photons with opposite OAM values are produced, placing an object in the path of one beam. We then present a classical (correlated, but nonentangled) version. The relative problems and benefits of the classical versus entangled configurations are discussed. The prospect is raised of carrying out compressive imaging via two-photon OAM detection to reconstruct sparse objects with few measurements.

DOI: 10.1103/PhysRevA.85.043825 PACS number(s): 42.50.Tx, 42.30.Va, 42.65.Lm

I. INTRODUCTION

In digital spiral imaging (DSI) [1], an object is illuminated by light with a known spatial phase distribution, or equivalently, of known orbital angular momentum (OAM) [2–4] distribution, and the OAM spectrum after the object is measured. The shape of the outgoing spectrum allows determination of some properties of the object, or possibly identification of the object from a known set. However, as we will see below, this method is incapable of reconstructing the actual shape of the object; despite its name, it is inherently a *nonimaging* technique.

Here, we propose *correlated spiral imaging* (CSI), measuring correlations of OAM values within two-photon states or between two light beams. We will consider measurement of the correlations both through coincidence counting and through interference between the two beams. We will then show that (i) the CSI coincidence rate displays clear signatures of object spatial properties, (ii) the mutual information carried by the detected pair has a strong dependence on object shape and measures the object's rotational symmetry, and (iii) a version of the setup *does* allow efficient reconstruction of object shape, opening up the possibility of carrying out compressive imaging with high-dimensional OAM states.

The experiments proposed here differ significantly from that carried out in Ref. [5]. In the latter, after filtering for specific OAM values, the spatial locations of the outgoing photons are measured in one arm, as in traditional ghost imaging [6–9]. But in the present case, *no* information about the spatial location or momentum of the photon is recorded; *only* angular momentum values are detected.

In the following sections, we describe two categories of correlated spiral imaging experiments, one involving entangled photon pairs produced via down-conversion, the other using classically correlated beams. The key point in all of the variations we describe is that there are *two* light beams (or two photons) with correlated OAM values. Our purposes here are twofold: both scientific and applied. On the pure science side, the entangled version is of great interest, following in a direct line from work such as that of [5,10], and offering a new window into both the down-conversion process and the quantum correlations between the signal and idler OAM values. The latter correlations are certainly of scientific interest in their own right, apart from any applications. On the applied side, the classical version is likely to be more useful, as discussed more fully in Sec. VI.

II. BACKGROUND

A. Laguerre-Gauss modes

We decompose ingoing and outgoing beams in terms of optical Laguerre-Gauss (LG) modes. The LG wave function with OAM $l\hbar$ and with p radial nodes is [11]

$$u_{lp}(r,z,\phi) = \frac{C_p^{|l|}}{w(z)}\left(\frac{\sqrt{2}r}{w(z)}\right)^{|l|} e^{-r^2/w^2(r)} L_p^{|l|}\left(\frac{2r^2}{w^2(r)}\right) \times e^{-ikr^2 z/[2(z^2+z_R^2)]} e^{-i\phi l + i(2p+|l|+1)\arctan(z/z_R)}, \quad (1)$$

with normalization $C_p^{|l|} = \sqrt{\frac{2p!}{\pi(p+|l|)!}}$ and beam radius $w(z) = w_0\sqrt{1+\frac{z}{z_R}}$ at z. $z_r = \frac{\pi w_0^2}{\lambda}$ is the Rayleigh range and the arctangent term is the Gouy phase.

B. Digital spiral imaging

DSI [1] is a form of angular momentum spectroscopy in which properties of an object are reconstructed based on how it alters the OAM spectrum of light used to illuminate it (Fig. 1). The input and output light may be expanded in LG functions, with the object acting by transforming the coefficients of the ingoing expansion into those of the outgoing expansion. Information about the transmission profiles of both phase and amplitude objects may be retrieved [1,12].

The idea naturally arises of trying to use the measured OAM spectrum to reconstruct an image of the object. But, although a great deal of information may be obtained about

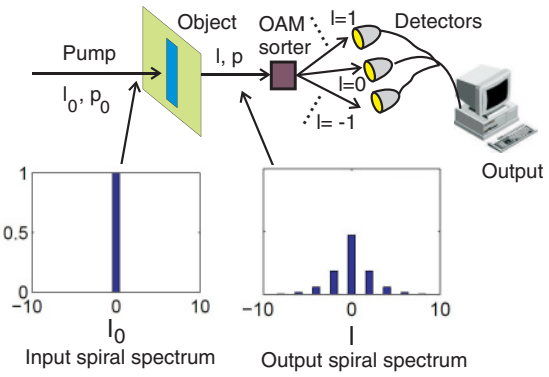

FIG. 1. (Color online) Digital spiral imaging: the presence of an object in the light beam alters the distribution of angular momentum values in the outgoing light.

the object in this manner, it is *not* sufficient to reconstruct a full image of the transmission or reflection profile. To see this, expand the output amplitude according to $\sum_{lp} A_{lp} u_{lp}$. Projecting out particular l and p values, the detector tells us the intensity of each component, allowing the $|A_{lp}|^2$ to be found, with no phase information retrieved. We thus have an incoherent imaging setup, with total detected intensity of the form $\sum_{lp} |A_{lp}|^2 |u_{lp}|^2$. But the quantities $|u_{lp}|^2$ are rotationally symmetric for all values of l and p (see the right-most panel of Fig. 2). Any image built from them is also symmetric; variation of the object about the axis is lost. In contrast, the real and imaginary parts are *not* rotationally invariant (left two panels of Fig. 2), so a coherent sum of the form $|\sum_{lp} A_{lp} u_{lp}|^2$ allows azimuthal structure to be reconstructed from the interference terms. For image reconstruction, we thus need to obtain a *coherent* superposition of amplitudes. This can be seen in Fig. 3: an opaque square is placed in the beam and the two expansions (coherent and incoherent) are computed, assuming that only the $p = 0$ components are measured and keeping terms up to $|l_{\max}| = 15$. In the left panel, where no phase information is assumed, the reconstructed image is rotationally invariant and there is no way to distinguish what the actual shape of the object was. In contrast, the coherent expansion on the right side of the figure produces a recognizably square output. *The phase information is vital in reconstructing the actual image shape*.

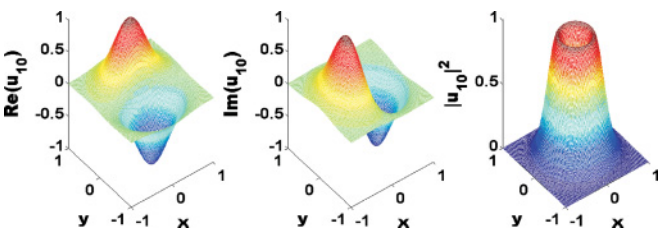

FIG. 2. (Color online) The real and imaginary parts of the Laguerre-Gauss function are not rotationally invariant, in contrast to its absolute square. This is illustrated for the case of $l = 1$, $p = 0$, but is true generally.

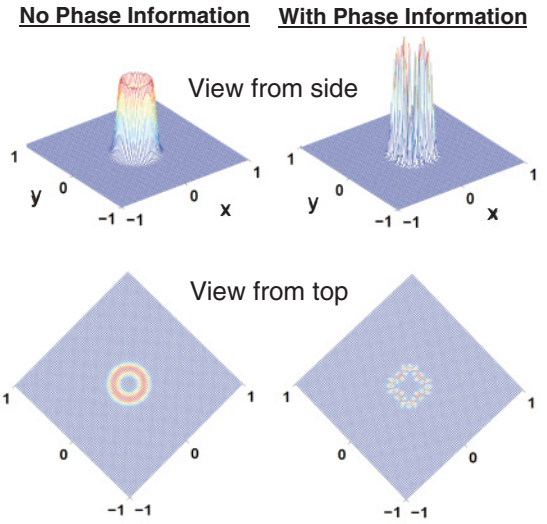

FIG. 3. (Color online) Incoherent (left) and coherent (right) expansions in Laguerre-Gauss functions, an opaque square object. In the former case, all variation of the object with angle around the axis is lost. ($p_{\max} = 0$ and $l_{\max} = 15$ assumed.)

C. Entangled OAM pairs

The form of the two-photon state produced by spontaneous parametric down-conversion (SPDC) is well known. It is most often written as an expansion in the space of transverse linear momenta of the outgoing signal and idler:

$$|\Psi\rangle = \int d^2q_s\, d^2q_i\, \tilde{E}(\boldsymbol{q}_s + \boldsymbol{q}_i)\tilde{W}(\boldsymbol{q}_s - \boldsymbol{q}_i)\hat{a}^\dagger_{q_s}\hat{a}^\dagger_{q_i}|0\rangle. \quad (2)$$

Here, $\tilde{E}$ is the momentum-space pump profile, and $\tilde{W}$ is the phase-matching function given by [13]

$$\tilde{W}(\boldsymbol{q}_s - \boldsymbol{q}_i) = \sqrt{\frac{2L}{\pi^2 k}}\,\mathrm{sinc}\left(\frac{|\boldsymbol{q}_s - \boldsymbol{q}_i|^2 L}{4k}\right) \times \exp\left(-i\frac{|\boldsymbol{q}_s - \boldsymbol{q}_i|^2 L}{4k}\right), \quad (3)$$

where L is the thickness of the crystal and $k = \frac{\omega_p n_p}{c}$ is the magnitude of the pump momentum.

In our case, however, we wish to expand in the space of orbital angular momentum instead of transverse linear momentum. Consider a pump beam of spatial profile $E(\boldsymbol{r}) = u_{l_0 p_0}(\boldsymbol{r})$ encountering a χ^2 nonlinear crystal, producing two outgoing beams via SPDC. For a fixed beam waist, the range of OAM values produced by the crystal is roughly inversely proportional to the square root of the crystal thickness L [12]. We wish a broad OAM bandwidth, so we assume a thin crystal located at the beam waist ($z = 0$). The output is an entangled state [10], with a superposition of terms of the form $u_{l'_1,p'_1} u_{l'_2,p'_2}$, angular momentum conservation requiring $l_0 = l'_1 + l'_2$. We will take the pump to have $l_0 = 0$, so that the OAM values just after the crystal are equal and opposite: $l'_1 = -l'_2 \equiv l$. The p'_1, p'_2 values are unconstrained, although the amplitudes drop rapidly with increasing p' values [see Eq. (6) below]. The output of the crystal may be expanded as a superposition of

signal and idler LG states:

$$|\Psi\rangle = \sum_{l_1',l_2'=-\infty}^{\infty} \sum_{p_1',p_2'=0}^{\infty} C_{p_1'p_2'}^{l_1',l_2'} |l_1',p_1';l_2',p_2'\rangle \delta(l_0 - l_1' - l_2'), \quad (4)$$

where the coupling coefficients are given by

$$C_{p_1'p_2'}^{l_1',l_2'} = \int d^2r \; \Phi(\boldsymbol{r}) \left[u_{l_1'p_1'}(\boldsymbol{r}) u_{l_2'p_2'}(\boldsymbol{r})\right]^*. \quad (5)$$

For the case of a pump beam with $l_0 = p_0 = 0$ this gives the coefficients [12,14]

$$C_{p_1,p_2}^{l,-l} = \sum_{m=0}^{p_1} \sum_{n=0}^{p_2} \left(\frac{2}{3}\right)^{m+n+l} (-1)^{m+n} \times \frac{\sqrt{p_1!p_2!(l+p_1)!(l+p_2)!}\,(l+m+n)!}{(p_1-m)!(p_2-n)!(l+m)!(l+n)!\,m!\,n!}. \quad (6)$$

III. JOINT OAM SPECTRA

We now investigate the use of two beams, rather than one, in combination with spiral imaging. The full benefits of doing this will emerge in Sec. V. In the current section, we focus on examination of the OAM correlations. We begin with an entangled version, where the light source is parametric down-conversion in a nonlinear crystal such as β-barium borate (BBO). Imagine an object in the signal beam (Fig. 4). Since OAM conservation holds exactly only in the paraxial case, we assume the signal and idler are produced in *collinear* down-conversion, then directed into separate branches by a beam splitter (BS). (Throughout this paper we assume all beam splitters are 50:50.) Assume perfect detectors for simplicity (imperfect detectors can be accounted for by the method in Ref. [14]). For our purposes, either type I down-conversion with a nonpolarizing beam splitter or type II with a polarizing beam splitter will work, since the processes involved are not polarization dependent. The only difference is that the use of type II with a polarizing beam splitter will increase the coincidence rate by a factor of 2. (Note that both photons enter the beam splitter through the same port, rather than through opposite ports, so there is no possibility of complete destructive interference of the kind that leads to the HOM dip.)

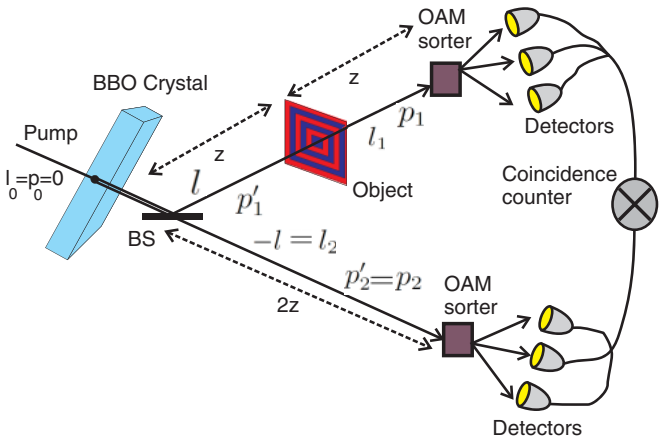

FIG. 4. (Color online) Setup for analyzing object via orbital angular momentum of entangled photon pairs.

Let $P(l_1,p_1;l_2,p_2)$ be the joint probability for detecting signal with quantum numbers l_1,p_1 and idler with values l_2,p_2. The marginal probabilities at the two detectors (probabilities for detection of a single photon, rather than for coincidence detection) are

$$P_s(l_1,p_1) = \sum_{l_2,p_2} P(l_1,p_1;l_2,p_2), \quad (7)$$

$$P_i(l_2,p_2) = \sum_{l_1,p_1} P(l_1,p_1;l_2,p_2). \quad (8)$$

Then the mutual information for the pair is

$$I(s,i) = \sum_{l_1,l_2=l_{\min}}^{l_{\max}} \sum_{p_1,p_2=0}^{p_{\max}} P(l_1,p_1;l_2,p_2) \times \log_2\left(\frac{P(l_1,p_1;l_2,p_2)}{P_s(l_1,p_1)P_i(l_2,p_2)}\right). \quad (9)$$

The most common experimental cases are when (i) the values of p_1 and p_2 are not measured (so all possible values of p_1 and p_2 must be summed, $p_{\max} = \infty$), or (ii) only the $p_1 = p_2 = 0$ modes are detected ($p_{\max} = 0$). Except when stated otherwise, we will use $l_{\max} = -l_{\min} = 10$ and $p_{\max} = 0$.

If the transmission function for the object is $T(\boldsymbol{x})$, the coincidence probabilities $P(l_1,p_1;l_2,p_2) = |A_{p_1p_2}^{l_1l_2}|^2$ have amplitudes

$$A_{p_1p_2}^{l_1l_2} = C_0 \sum_{p_1'} C_{p_1'p_2}^{-l_2,l_2} a_{p_1'p_1}^{-l_2,l_1}(z), \quad (10)$$

$$a_{p_1'p_1}^{l_1'l_1}(z) = \int u_{l_1'p_1'}(\boldsymbol{x},z)\left[u_{l_1p_1}(\boldsymbol{x},z)\right]^* T(\boldsymbol{x}) d^2x, \quad (11)$$

where C_0 is a normalization constant. Here it is assumed that the total distance in each branch is $2z$ (see Fig. 4).

That the object's size and shape affect the coincidence rate is easy to see. For example, Fig. 5 shows the calculated spectrum when a single opaque strip of width d is placed in the beam. Figure 6 shows the corresponding mutual information, assuming that only the $p_1 = p_2 = 0$ component is detected. In both figures, we see clear effects of changing an object parameter (the strip width).

The central peak of the spectrum (Fig. 5) broadens as d increases from zero, reducing the correlation between l_1 and l_2; the mutual information between them thus declines, as seen in the $d/w_0 < 1$ portion of Fig. 6. But at $d/w_0 \approx 1$, the central peak in $\{l_1,l_2\}$ space bifurcates into two narrower peaks (right side of Fig. 5); the information thus goes back up as the

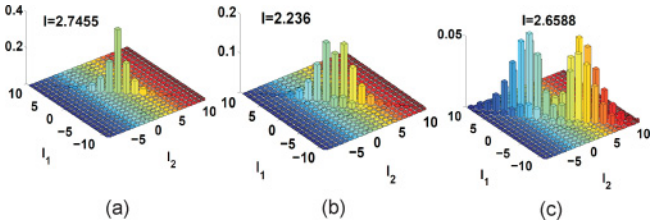

FIG. 5. (Color online) An opaque strip of width d placed in the signal path. The widths are (a) $d = 0.1w_0$, (b) $d = 0.9w_0$, and (c) $d = 2.5w_0$. The outgoing joint angular momentum spectra are plotted. As the width increases, the peak in the spectrum broadens, then (at $d = w_0$) splits into two peaks.

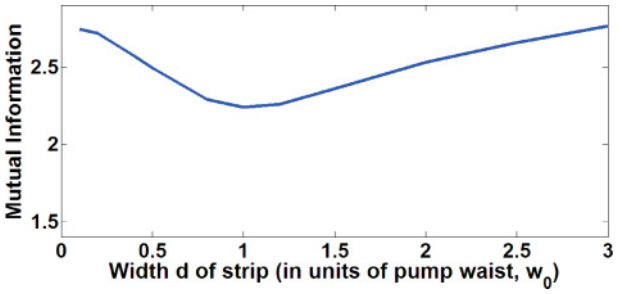

FIG. 6. (Color online) Mutual information vs width of opaque strip. The horizontal axis is in units of w_0. The minimum information occurs at $d = w_0$.

peaks separate, as indeed is the case in the $d/w_0 > 1$ region of Fig. 6. If we continue to wider d, the two peaks once again broaden and the mutual information decays gradually to zero. In addition, the total intensity getting past the opaque strip will continue to drop, so coincidence counts decay rapidly.

IV. MUTUAL INFORMATION AND SYMMETRY

Figure 7 shows the computed mutual information for several simple shapes. It can be seen that I depends strongly on the size and shape of the object, so that for object identification from among a small set a comparison of the I values rather than of the full probability distribution may suffice.

If the object has rotational symmetry about the pump axis, then its transmission function $T(r)$ depends only on radial distance r, not on azimuthal angle ϕ. The angular integral in Eq. (11) is then $\int_0^{2\pi} e^{-i\phi(l-l')}d\phi = 2\pi\delta_{l,l'}$. So the joint probabilities reduce to the form $P(l_1,l_2) = f(l_1)\delta_{l_1,l_2}$ (assuming $p_1 = p_2 = 0$) for some function f. The marginal probabilities for each arm reduce to $P_1(l_1) = f(l_1)$ and $P_2(l_2) = f(l_2)$. The mutual information $I(L_1,L_2) = S_1(L_1)$ where $S_1(L_1) = -\sum_{l_1} f(l_1)\ln f(l_1)$ is the Shannon information of the object arm OAM spectrum. Thus in the case of rotational symmetry, the second arm becomes irrelevant from an information standpoint. In this sense, the quantity $\mu(L_1,L_2) \equiv |I(L_1,L_2) - S_1(L_1)|$ is an order parameter, capable of detecting breaking of rotational symmetry.

More generally, suppose that the object has a rotational symmetry group of order N; i.e., it is invariant under $\phi \to \phi + \frac{2\pi}{N}$. From Eqs. (1) and (11) it follows that the coefficients must then satisfy $a^{l_1' l_1}_{p_1' p_1} = e^{\frac{2\pi i}{N}(l_1'-l_1)} a^{l_1' l_1}_{p_1' p_1}$, which implies $a^{l_1' l_1}_{p_1' p_1} = 0$ except when $\frac{l_1'-l_1}{N}$ is an integer. When N goes up (enlarged symmetry group), the number of nonzero $a^{l_1' l_1}_{p_1' p_1}$ goes down; with the probability concentrated in a smaller number of configurations, correlations increase and mutual information goes up. This may be seen in the three right-most objects of Fig. 7, for example.

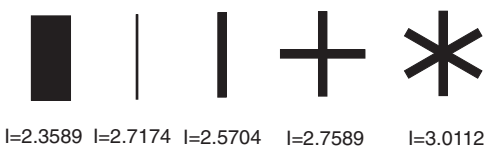

FIG. 7. (Color online) The mutual information depends strongly on size and shape of the object. Here, the two objects on the left have widths $1.5w_0$ and $0.2w_0$; all other widths are $0.4w_0$.

V. IMAGING

The inability of DSI to produce images due to loss of phase information has been pointed out. Here we show that a variation on the entangled CSI setup can be used to find the expansion coefficients *including phase*.

First, we note from Eq. (6) that the factors $C^{l_1',l_2'}_{p_1' p_2'}$ are real and positive, so the phases of the amplitudes $A^{l_1 l_2}_{p_1 p_2}$ are entirely determined by the phases of the $a^{-l_2,l_1}_{p_1' p_1}(z)$. Note further from Eqs. (1) and (11) that the only p dependence in the phase of $a^{-l_2,l_1}_{p_1' p_1}(z)$ is in the factor $e^{-2ip\psi(z)}$, where $\psi(z) = \arctan\frac{z}{z_R}$. If z is much greater than z_R, then $\psi \approx \frac{\pi}{2}$ is roughly constant, so that $e^{-2ip\psi(z)} \approx (-1)^p$. Since we assume the outgoing p values are $p_1 = p_2 = 0$, the relevant detection amplitude is

$$A^{l_1 l_2}_{00} = \sum_{p_1'} C^{-l_2,l_2}_{p_1' 0} a^{-l_2,l_1}_{p_1' 0} \approx C^{-l_2,l_2}_{00} a^{-l_2,l_1}_{00} + C^{-l_2,l_2}_{10} a^{-l_2,l_1}_{10}, \tag{12}$$

due to rapid decay of the $C^{-l_2,l_2}_{p_1' 0}$ with increasing $|p_1' - p_1|$. So if we break $a^{-l_2,l_1}_{p_1' 0}$ into amplitude and phase, $a^{-l_2,l_1}_{p_1' 0} = r^{-l_2,l_1}_{p_1'} e^{i\phi_{p_1' l_1 l_2}}$, then the phase is independent of p_1', except for a relative minus sign between even and odd p_1' terms, so that

$$A^{l_1 l_2}_{00} = \rho_{l_1,l_2} e^{i\phi_{l_1 l_2}}, \tag{13}$$

where $\phi_{l_1 l_2}$ is the value of $\phi_{p_1' l_1 l_2}$ for even p_1', and $\rho_{l_1 l_2} \equiv (C^{-l_2,l_2}_{00} - C^{-l_2,l_2}_{10}) r^{-l_2,l_1}_0$ is real and positive. Thus, the phase of $A^{l_1 l_2}_{00}$ is the same as the phase of $a_{p_1' 0}$ for even p_1' and differs from that of $a_{p_1' 0}$ by a factor of π for p_1' odd. Finding the phases of the coincidence detection amplitudes $A^{l_1 l_2}_{00}$ therefore suffices to determine the phases of all of the $a_{p_1' 0}$ coefficients.

The measurement of these phases is accomplished by inserting a beam splitter to mix the signal and idler beams before detection, as in Fig. 8, erasing information about which photon followed which path. We then count singles rates in the two detection stages, rather than the coincidence rate. If value l is detected at a given detector it could have arrived by two different paths, so interference occurs between these two possibilities. The detection amplitudes

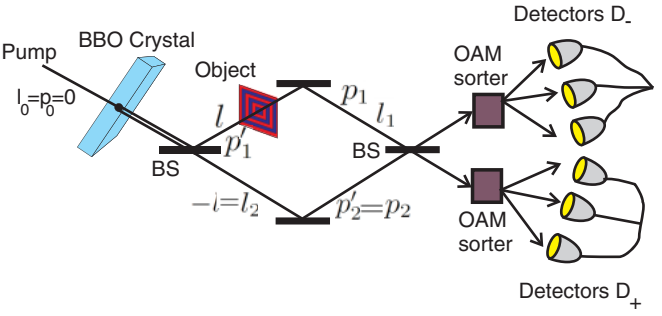

FIG. 8. (Color online) A configuration allowing image reconstruction via phase-sensitive measurement of entangled OAM content.

in the two sets of detectors D_+ and D_- involve factors $A_+ \sim (1 + i a_{00}^{l_0-l_2,l_1})$ and $A_- \sim (i + a_{00}^{l_0-l_2,l_1})$, with detection rates $R_\pm \sim 1 + |a_{00}^{l_0-l_2,l_1}|^2 \pm 2i \,\mathrm{Im}\, a_{00}^{l_0-l_2,l_1}$. From these counting rates, both the amplitudes and the relative phases of all coefficients can be found, allowing full image reconstruction.

Once the coefficients $a_{p_1',p_1}^{l_1',l_1}$ have been found from the coincidence rates, image reconstruction requires the inversion of Eq. (11) to find the object transmission function $T(\boldsymbol{r})$. To facilitate this, we first define an operator $\hat{T}$ to represent the effect of the object on the beam. We may expand this operator in the position basis,

$$\hat{T} = \int d^2r \; d^2r' |\boldsymbol{r}'\rangle T(\boldsymbol{r},\boldsymbol{r}') \langle \boldsymbol{r}| \tag{14}$$

$$= \int d^2r \; |\boldsymbol{r}\rangle T(\boldsymbol{r}) \langle \boldsymbol{r}|, \tag{15}$$

where in the last line we assumed that the operator is a local operator, diagonal in the position space basis. The object function $T(\boldsymbol{r})$ in Eq. (11) is then given by

$$T(\boldsymbol{r}) = \langle \boldsymbol{r}|\hat{T}|\boldsymbol{r}\rangle. \tag{16}$$

Alternatively, the object operator may be expanded in the Laguerre-Gauss basis,

$$\hat{T} = \sum_{ll'} \sum_{pp'} d_{p'p}^{l'l} \; |l'p'\rangle\langle lp|. \tag{17}$$

Making use of these definitions and of Eq. (11), it follows immediately that

$$d_{p_1',p_1}^{l_1',l_1} = \langle l_1' p_1' |\hat{T}| l_1 p_1 \rangle = a_{p_1,p_1'}^{l_1,l_1'}. \tag{18}$$

(Note the reversal in the order of the indices.) Using this result in Eq. (17), then applying Eq. (16) and the fact that

$$u_{lp}(\boldsymbol{r}) = \langle \boldsymbol{r}|lp\rangle, \tag{19}$$

we find that determination of the $a_{p_1',p_1}^{l_1',l_1}$ coefficients is equivalent to reconstructing the object, since

$$T(\boldsymbol{r}) = \langle \boldsymbol{r}|\hat{T}|\boldsymbol{r}\rangle = \sum_{ll'} \sum_{pp'} a_{p_1',p_1}^{l_1',l_1} u_{l_1 p_1}(\boldsymbol{r}) \left[u_{l_1' p_1'}(\boldsymbol{r})\right]^*. \tag{20}$$

An example is shown in Fig. 9, in which the object composed of a single opaque band of the type used in the simulations of Sec. III (strip width is equal to 0.5 times the beam waist) is reconstructed using Eq. (20) for different values of $l_{\max}$ and $p_{\max}$. We see that as the number of values of l included is increased, a valley appears in the transmission profile at the location of the opaque band, and gradually becomes sharper and more pronounced as we increase $l_{\max}$.

Note for reference in Sec. VII below that in the previous example, only $(2l_{\max} + 1)p_{\max} = 76$ measurements are needed to reconstruct the bottom 60×60 pixel image, yet the result is already a reasonably good approximation to the original object.

VI. CLASSICAL CSI

In recent years, it has been shown that ghost imaging and other "quantum" two-photon effects may be carried out using classically correlated sources [15–20]. It is apparent that the same is true in the case of correlated spiral imaging: classical OAM correlation, rather than entanglement, is sufficient. The essential point in the present case is having two spatially separated beams such that if the OAM detected in one beam is known, then the OAM reaching the object can be predicted. So all that is needed is strong classical correlation or anticorrelation between the OAM in the two arms.

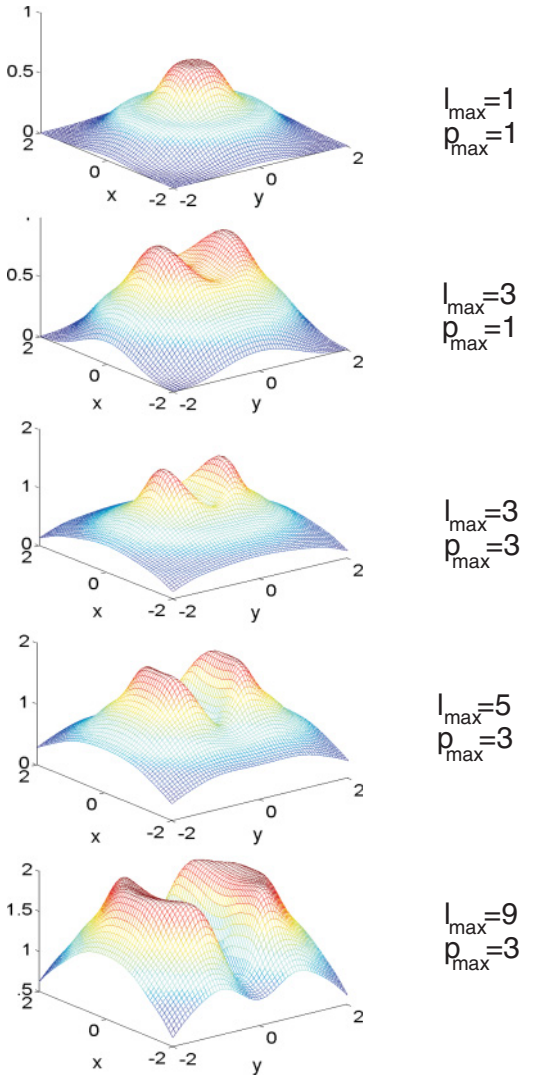

FIG. 9. (Color online) Reconstruction of the transmission profile of an object with a single opaque band of width $0.5w_0$ for several values of $l_{\max}$ and $p_{\max}$. We see the shape of the object appear and begin to sharpen as more l and p values are included.

The classical analog of apparatus of Fig. 8 is shown in Fig. 10. At the left, the system is illuminated with light that has a broad range of OAM values (a broad spiral spectrum). The beam is split, with one copy passing through the object, and the other entering the reference branch. The two beams are mixed at the beam splitter, then the OAM content at the two detectors is measured. The coefficients $C_{p_1,p_2}^{l_1,l_2}$ will no longer be given by Eq. (6), but instead will have values determined by the properties of the specific input beam being used. The mutual information between the classical beams may be defined just as in Eq. (9).

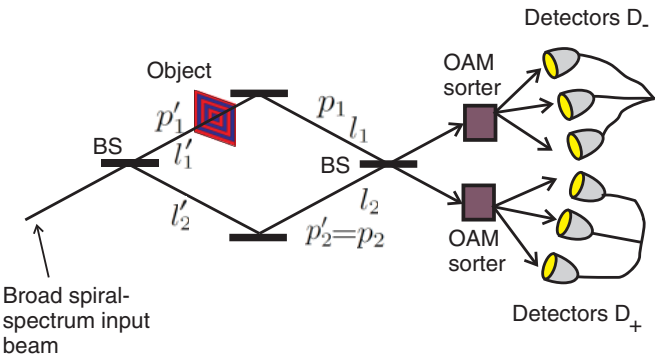

FIG. 10. (Color online) A classical version of correlated spiral imaging. An input beam with a broad range of OAM values is split at a beam splitter, sending a portion through the reference branch, and the rest to the object.

The classical configuration of CSI has a number of practical advantages over the entangled version: alignment issues are greatly reduced, single photon detectors are not needed, and much higher brightness and counting rate may be obtained. There is one problem that arises, however, which is not present in the entangled case: if a broad spiral spectrum is used for the illumination, then there is no intrinsic correlation between the OAM value l_2 in the reference branch and the value l_1' that occurs between the source and object. Without this correlation, the value of l_1' is unknown and so the change in l produced by the object is also unknown. On the other hand, instead of a broad spiral spectrum, we may send in single OAM values, one at a time, building up the OAM correlation function one value of l_1' at a time. But this slows the process of image reconstruction considerably: a range of OAM values needs to be scanned over, one after another, changing a spiral phase plate or some other type of OAM filter multiple times in each run. In a kind of quantum parallelism, the entangled version can send in a broad range of values simultaneously, and the entangled nature of the source will automatically ensure that the pairs detected are of opposite initial OAM if a short enough coincidence time window is used. In any case, whether the classical or entangled version is used, two correlated beams are necessary in order to reconstruct the relative phases of the various OAM amplitudes.

VII. COMPRESSIVE IMAGING

Recent years have shown an explosion of interest in compressive sensing [21–25], including compressive ghost imaging [26]. The basic idea is that most images are very sparse when expanded in an appropriate basis, with the vast majority of expansion coefficients being very small. So if a sampling procedure is used that only measures the relatively small number of large expansion coefficients and neglects the rest, the image may be reconstructed from a very small number of measurements, often much smaller than naively expected from the Shannon-Nyquist theorem.

The joint OAM spectra (such as those shown in Fig. 5) have been calculated for a variety of other opaque objects of various shapes, and in all of them it has been found that only a relatively small number of the coefficients have significant amplitude. Recall also that in the example associated with Fig. 9 the images shown were reconstructed using the values of far fewer amplitudes than there were pixels in the reconstruction. The LG functions can therefore serve as a sparse basis for these simple shapes. It is likely that this will also be true of at least some classes of more complex objects. The possibility thus opens of compressive imaging with OAM states by the CSI method. Only two additional ingredients are needed: (i) Instead of taking $l_0 = 0$, as we did in Sec. III, we should illuminate the crystal with a broad range of l_0, providing a large number of randomly occurring input states; this provides the large number of randomly chosen sampling bases needed for compressive imaging. (ii) The basis used for sensing (LG basis, $|l, p\rangle$) and that used to reconstruct the image (position basis $|\boldsymbol{r}\rangle$) should have low mutual coherence [21,25]; this means the maximum value of $|\langle \boldsymbol{r}|lp\rangle| = |u_{lp}(\boldsymbol{r})|$ should be as small as possible, implying that the range of l and p values used should be centered at the largest possible mean value.

The combined requirements of high mean l and large spread in l are easily satisfied. If a pump beam of OAM l_0 is used, the signal and idler will each have mean value $l_0/2$, so a pump beam of high angular momentum will lead to satisfaction of the first condition. The second condition can be satisfied by placing an obstruction in the path of the pump which blocks all light except that passing through an angular aperture of narrow angle $\Delta\phi$ (see Fig. 11). Since l and ϕ are conjugate variables, restricting the values of ϕ causes spreading of the l values [27], allowing the second condition to be satisfied. Alternatively, a wider pump beam and thinner crystal can also broaden the OAM bandwidth.

To briefly review compressive imaging, we start by imagining that we wish to measure some signal s. In our case, s will be a vector specifying how the signal is distributed in the detection plane, from which we wish to reconstruct an image. We consider expansion of the signal $|s\rangle$ and our reconstructed image $|i\rangle$ in two different bases:

$$|s\rangle = \text{signal} = \sum_{lp} d_{lp}|lp\rangle, \tag{21}$$

$$|i\rangle = \text{image} = \sum_{k} c_k|\psi_k\rangle. \tag{22}$$

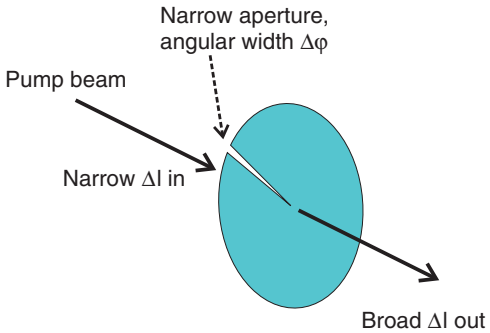

FIG. 11. (Color online) An aperture allowing passage of only a narrow range of angles about the propagation axis causes a spread in the outgoing OAM values.

Here, the Laguerre-Gauss basis, spanned by the $|lp\rangle$ basis vectors, will be our *measurement basis*: we sample the signal by measuring M projections

$$y_{lp} = \langle s|lp\rangle \in \{d_{lp}\} \tag{23}$$

onto a randomly selected collection of the basis vectors, $\{l_1, p_1\}, \ldots, \{l_M, p_M\}$. The second basis, consisting of the N vectors $|\psi_k\rangle$ is the *reconstruction basis*: we build our final image as a linear combination of these basis vectors. Compressive imaging then consists of measuring the M sample values y_{lp} in the $|lp\rangle$ basis, then minimizing the L^1 norm of the $|\psi_k\rangle$ expansion,

$$\sum_k |c_k| = \text{ minimum}, \tag{24}$$

subject to the M constraints

$$y_{lp} = \sum_k c_k^* \langle \psi_k|l, p\rangle. \tag{25}$$

This reflects the requirement that the reconstructed image be consistent with the sampled data, or in other words, the requirement that $y_{lp} = \langle i|lp\rangle$. The bases should be chosen to have a high degree of mutual incoherence, meaning that the maximum value of $\langle \psi_k|l, p\rangle$ should be small. The incoherence requirement means that each $|lp\rangle$ state overlaps with many $|\psi_k\rangle$, and thus samples many of them simultaneously.

To construct an image, the simplest choice for the reconstruction basis is a discretized position basis; in other words, $\psi_k = \boldsymbol{x}_k$ is taken to be the position of the kth pixel. The overlap between the kth element of position basis and the l, p element of the OAM basis is given by the Laguerre-Gauss function at the location of the kth pixel, $\langle \psi_k|l, p\rangle = \langle \boldsymbol{x}_k|l, p\rangle = u_{lp}(\boldsymbol{x}_k)$; the degree of coherence for an image containing n pixels is then defined to be

$$\mu = \sqrt{n}\, \max_{l,p,k} u_{lp}(\boldsymbol{x}_k), \tag{26}$$

where $\max_{l,p,k}$ means to maximize over all values of l, p, and k. The degree of coherence, which is always between 1 and $\sqrt{n}$, should be as close to 1 as possible for maximum compressibility. As shown in Fig. 12, for an image on an $n \times n$ array of pixels the coherence between the LG and position bases converges rapidly to $\mu = 2.407$ as n increases.

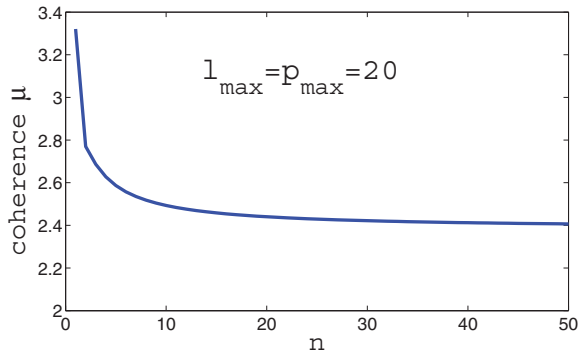

FIG. 12. (Color online) The coherence between the position and Laguerre-Gauss basis for an image displayed on an $n \times n$ square array of pixels. The coherence drops rapidly with increasing n for small n values, then converges rapidly to a value of $\mu = 2.407$.

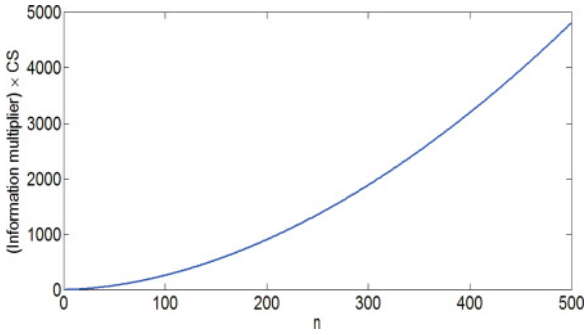

FIG. 13. (Color online) The ratio of number of pixels (n^2) to number of OAM measurements needed for exact image reconstruction ($CS\mu^2 \log_2 n$) plotted in units of $1/CS$.

The image can then be reconstructed exactly with overwhelming probability if the number of samples M (the number of l, p combinations measured) satisfies

$$M > CS\mu^2 \log_2 n, \tag{27}$$

where S is the sparsity of the image [the number of coefficients in Eq. (21) which are not negligibly small] and C is a constant. Specifically, if inequality (27) is satisfied, then the probability of successful imaging with M samples is greater than $1 - M^{-\delta}$, where $\delta = \frac{C}{22} - 1$ [21]. δ should be positive, so C should always be taken to be larger than 22.

For an object of sparseness S in the OAM basis and coherence μ used to reconstruct an $n \times n$-pixel image, the information normally carried by a minimum number n^2 of photons can instead be obtained from a number of photons on the order of $CS\mu^2 \log_2 n$. This situation can be interpreted as extracting from each photon an effective amount of information that is larger than normal by a factor on the order of $n^2/(CS\mu^2 \log_2 n)$. This multiplication factor is plotted in Fig. 13; we see that even if CS is on the order of several hundred, the information gain per photon increases with n and is significant for $n \times n$ arrays of pixels of realistic size (n greater than a few hundred).

VIII. CONCLUSION

We have shown that correlations between the orbital angular momentum of correlated or entangled photon pairs can carry information about the size and shape of an object. A procedure has been described for using this information for image reconstruction and arguments have been given to believe that compressive imaging can be productively carried out with OAM correlations.

It is easy to envision a number of variations on the configurations of the current paper that may be worth exploring in the future. One example is "ghost" spiral imaging, where the OAM sorter is removed from the object arm and the l_1 values are not measured at all (analogous to having a bucket detector in ordinary ghost imaging). That signatures of the

object will still appear can easily be seen by imagining taking the sum over the l_1 rows in the histograms of Fig. 5: it is immediately obvious that the resulting distributions still vary from one object to the next.

ACKNOWLEDGMENT

This research was supported by the DARPA InPho program through US Army Research Office award W911NF-10-1-0404.

[1] L. Torner, J. P. Torres, and S. Carrasco, Opt. Express **13**, 873 (2005); G. Molina-Terriza, L. Rebane, J. P. Torres, L. Torner, and S. Carrasco, J. Eur. Opt. Soc. **2**, 07014 (2007).

[2] L. Allen, M. W. Beijersbergen, R. J. C. Spreeuw, and J. P. Woerdman, Phys. Rev. A **45**, 8185 (1992).

[3] S. Franke-Arnold, L. Allen, and M. Padgett, Laser Photonics Rev. **2**, 299 (2008).

[4] A. M. Yao and M. J. Padgett, Adv. Opt. Photonics **3**, 161 (2011).

[5] B. Jack, J. Leach, J. Romero, S. Franke-Arnold, M. Ritsch-Marte, S. M. Barnett, and M. J. Padgett, Phys. Rev. Lett. **103**, 083602 (2009).

[6] D. N. Klyshko, Zh. Eksp. Teor. Fiz. **94**, 82 (1988) [Sov. Phys. JETP **67**, 1131 (1988)].

[7] A. V. Belinskii and D. N. Klyshko, Zh. Eksp. Teor. Fiz. **105**, 487 (1994) [Sov. Phys. JETP **78**, 259 (1994)].

[8] T. B. Pittman, Y. H. Shih, D. V. Strekalov, and A. V. Sergienko, Phys. Rev. A **52**, R3429 (1995).

[9] D. V. Strekalov, A. V. Sergienko, D. N. Klyshko, and Y. H. Shih, Phys. Rev. Lett. **74**, 3600 (1995).

[10] A. Mair, A. Vaziri, G. Weihs, and A. Zeilinger, Nature **412**, 313 (2001).

[11] L. Allen, M. Padgett, and M. Babiker, Prog. Opt. **39**, 291 (1999).

[12] J. P. Torres, A. Alexandrescu, and L. Torner, Phys. Rev. A **68**, 050301(R) (2003).

[13] B. E. A. Saleh, A. F. Abouraddy, A. V. Sergienko, and M. C. Teich, Phys. Rev. A **62**, 043816 (2000).

[14] X. F. Ren, G. P. Guo, B. Yu, J. Li, and G. C. Guo, J. Opt. B **6**, 243 (2004).

[15] R. S. Bennink, S. J. Bentley, and R. W. Boyd, Phys. Rev. Lett. **89**, 113601 (2002).

[16] R. S. Bennink, S. J. Bentley, R. W. Boyd, and J. C. Howell, Phys. Rev. Lett. **92**, 033601 (2004).

[17] A. Gatti, E. Brambilla, M. Bache, and L. A. Lugiato, Phys. Rev. Lett. **93**, 093602 (2004).

[18] A. Valencia, G. Scarcelli, M. D'Angelo, and Y. H. Shih, Phys. Rev. Lett. **94**, 063601 (2005).

[19] G. Scarcelli, V. Berardi, and Y. H. Shih, Phys. Rev. Lett. **96**, 063602 (2006).

[20] F. Ferri, D. Magatti, A. Gatti, M. Bache, E. Brambilla, and L. A. Lugiato, Phys. Rev. Lett. **94**, 183602 (2005).

[21] E. J. Candès, in *Proceedings of the International Congress of Mathematicians Madrid, August 2230, 2006*, edited by M. Sanz-Solé, J. Soria, J. L. Varona, and J. Verdera (EMS Publishing, Zurich, 2007).

[22] E. J. Candès, J. Romberg, and T. Tao, IEEE Trans. Inf. Theory **52**, 489 (2006).

[23] E. J. Candès and T. Tao, IEEE Trans. Inf. Theory **52**, 5406 (2006).

[24] D. Donoho, IEEE Trans. Inf. Theory **52**, 1289 (2006).

[25] E. J. Candès and M. B. Wakin, IEEE Signal Process. Mag. 21 (2008).

[26] O. Katz, Y. Bromberg, and Y. Silberberg, Appl. Phys. Lett. **95**, 113110 (2009).

[27] B. Jack, P. Aursand, S. Franke-Arnold, D. G. Ireland, J. Leach, S. M. Barnett, and M. J. Padgett, J. Opt. **13**, 064017 (2011).